Available online at www.sciencedirect.com
ScienceDirect
Catalysis Communications 8 (2007) 971–976
CATALYSIS COMMUNICATIONS
www.elsevier.com/locate/catcom

An integrated low temperature approach to highly photoactive nanocrystalline mesostructured titania

Jian Zhu [a], Zhen-Feng Bian [b], Jie Ren [b], Yong-Mei Liu [a], Yong Cao [a,*], He-Xing Li [b], Wei-Lin Dai [a], He-Yong He [a], Kang-Nian Fan [a,*]

[a] *Department of Chemistry and Shanghai Key Laboratory of Molecular Catalysis and Innovative Materials, Fudan University, No. 220#, Handan Road, Shanghai 200433, PR China*
[b] *Department of Chemistry, Shanghai Normal University, Shanghai 200234, PR China*

Received 2 June 2006; received in revised form 28 July 2006; accepted 21 August 2006
Available online 3 September 2006

Abstract

A new type of nanocrystalline mesostructured TiO_2 (NMT) predominantly in the anatase phase with a high specific surface area up to 269 $m^2\ g^{-1}$ was prepared by a novel integrated nonhydrolytic sol–gel/UV-illumination technique at low temperature. During the gaseous phase photocatalytic degradation of acetone, the material exhibited excellent photoactivity, much higher than commercial Degussa P-25, which closely related to the markedly enhanced crystallization degree and the beneficial formation of surface Ti–OH groups on the NMT sample during the post UV-illumination process.

Keywords: Nanocrystalline mesostructured TiO_2; Anatase; UV-illumination; Low temperature; Nonhydrolytic sol–gel

1. Introduction

Nanocrystalline titanium dioxide (TiO_2) has attracted considerable recent attention as one of the key materials for applications in many technologies, including photocatalysis, solar energy conversion, and ductile ceramics [1,2]. The specific surface area and crystallinity of TiO_2 nanocrystallites are two of the most important factors affecting their structural and functional properties such as light absorbing, electrical, adsorption behavior, and photocatalytic activity [3–5]. Despite a large number of synthetic methods such as sol–gel reactions (based on both hydrolytic and nonhydrolytic reaction pathways) and microemulsions have been developed for the preparation of TiO_2, the materials obtained are amorphous or semicrystalline titania [6–9]. Hydrothermal processing or subsequent calcination is required to induce crystallization of the nanoparticles, which however leads to undesirable sintering, grain growth, and dramatic loss of specific surface area in many cases [10–12]. In this respect, the seeking of new versatile low-temperature routes to nanocrystalline anatase TiO_2 photocatalysts with favorable structural and functional properties is still an open challenge.

In this letter, we report a practical and convenient method to prepare nanocrystalline mesostructured TiO_2 (NMT) predominantly in the anatase phase with a high specific surface area at low temperatures (60–80 °C). We also demonstrate that the as-prepared nanocrystalline NMT material exhibits excellent photoefficiency far exceeding that of commercial Degussa P-25 during the gaseous phase photocatalytic degradation of acetone. The approach utilized in the present work is based on an integrated nonhydrolytic sol–gel/UV-illumination technique utilizing $TiCl_4$ and *tert*-butyl alcohol as starting materials. Whereas the conventional nonhydrolytic sol–gel (NSG) derived TiO_2 nanocrystals are frequently associated with significant amount of organic species and semicrystalline

* Corresponding authors. Tel.: +86 21 65643977/656437925; fax: +86 21 65642978.
E-mail addresses: yongcao@fudan.edu.cn (Y. Cao), knfan@fudan.edu.cn (K.-N. Fan).

1566-7367/$ - see front matter © 2006 Elsevier B.V. All rights reserved.
doi:10.1016/j.catcom.2006.08.030

in nature thus not suitable for many technological applications [8,13], the present integrated process can readily allow the fabrication of "surface-clean" nanocrystalline mesostructured TiO_2 (NMT) materials possessing well-crystallized anatase phase and high surface area.

2. Experimental

2.1. Catalyst preparation

The present integrated preparation of nanocrystalline TiO_2 at low temperatures consists of two consecutive synthetic procedures involving the nonhydrolytic sol–gel process followed by a post UV-illumination treatment. The nonhydrolytic sol–gel process utilized in this study is based on a previously reported "alkyl halide elimination" route developed by Vioux et al. [9]. Briefly, 2 ml $TiCl_4$ was added dropwise into 20 ml pure *tert*-butyl alcohol solution (Aldrich, 99.9%) at 30 °C under vigorous stirring with the protection of argon flow (20 ml/min). After continuous stirring for 3 h followed by maintaining the resulting clear sol under static conditions at a higher temperature of 60 °C for another 12 h, a translucent off-white alcogel was obtained. The resultant alcogel was then air dried at 80 °C for 12 h. The collected material (labeled as NMT-AS, brown in color) was then subjected to subsequent UV-illumination treatment in a self-constructed fluidized bed photoreactor, where a high pressure Hg-light (365 nm, 150 W) was used as the UV-source, for a short time of 30–100 min to obtain the final UV-illuminated nanocrystalline mesostructured TiO_2 samples, referred to herein as NMT-*t* (*t* denotes the time of the UV processing, Table 1).

2.2. Catalyst characterization

The textural parameters have been measured using the BET method by N_2 adsorption and desorption at 77 K in a Micromeritics TriStar system. Transmission electron micrographs (TEM) were recorded digitally with a Gatan slow-scan charge-coupled device (CCD) camera on a JEOL 2011 electron microscope operating at 200 kV. The samples for electron microscopy were prepared by grinding and subsequent dispersing the powder in acetone and applying a drop of very dilute suspension on carbon-coated grids. The X-ray powder diffraction (XRD) of the samples was carried out on a Germany Bruker D8Advance X-ray diffractometer using nickel filtered Cu Kα radiation with a scanning angle (2θ) of 10–80°, and a voltage and current of 40 kV and 20 mA. The average size of anatase TiO_2 crystallites was estimated by means of the Scherrer equation from broadening of the (1 0 1) anatase reflection. Estimation of the content of anatase is based on: $X_A = 1/[1 + 1.265\, I_R/I_A] \times 100\%$, where I_A is the (1 0 1) peak intensity of anatase, I_R is the (1 1 0) peak intensity of rutile, and 1.265 is the scattering coefficient. X-ray photoelectron spectroscopy (XPS) spectra were recorded with a Perkin–Elmer PHI 5000 C system equipped with a hemispherical electron energy analyzer. The spectrometer was operated at 15 kV and 20 mA, and an aluminum anode (Al Kα, $\hbar\nu = 1486.6$ eV) was used. The C 1s line (284.6 eV) was used as the reference to calculate the binding energies (BE).

2.3. Catalytic tests

The photocatalytic degradation of acetone was performed by measuring the gaseous concentration of acetone as a function of the irradiation time in a Pyrex glass reactor interfaced with quartz window with a capacity of 7 L. For each experiment, about 0.1 g catalysts were dispersed in a sample platform with irradiation area of 113 cm^2. The initial concentration of acetone after reaching adsorption/desorption equilibrium was 1500 ± 5 μL/L and four 8 W UV lamps (λ: 310 nm) were used as light source. During the overall degradation process, the temperature was controlled at ca. 40 ± 1 °C. The gaseous products were measured by an on-line GC (Agilent 6820), which shows a near 3:1 ratio of carbon dioxide products to decreased acetone. The measurements were repeated for each catalyst and the experimental error was found to be within ±3%.

3. Results and discussion

The XRD measurements reveal that the as-synthesized NMT-AS sample underwent interesting microstructural evolution during the UV-illumination process. As shown

Table 1
Physico-chemical characteristics of various NMT samples

Samples	S_{BET}[a] ($m^2\ g^{-1}$)	V_p[a] ($cm^3\ g^{-1}$)	D_p[a] (nm)	Crystallite size[b] (nm)	Crystallinity[c] (%)	O_{OH}/O_T[d] (%)	Organic residues (mass%)[e]
NMT-AS	188	0.23	3.9	4.7	46	19	12
NMT-30	229	0.26	4.3	5.4	59	27	5
NMT-50	259	0.30	4.5	5.7	85	38	1.7
NMT-100	269	0.31	4.6	6.0	90	40	0.6
P-25[f]	55	0.21	/	25	/	26	/

[a] BET surface area (S_{BET}), average pore volume (V_p) and average pore diameter (D_p) of the NMT samples estimated from nitrogen adsorption.
[b] Average crystallite size of anatase TiO_2 nanoparticles estimated from Scherrer equation.
[c] Relative anatase crystallinity measured according to literature procedure [14].
[d] Ratio of O_{OH} and O_T was calculated from area integral of O_{OH} and O_L in O 1s XPS spectra ($O_T = O_{OH} + O_L$) [18].
[e] The content of carbonaceous residues in the samples obtained from the TG data based on the weight loss between 200 and 700 °C [21].
[f] Commercial photocatalyst Degussa P-25.

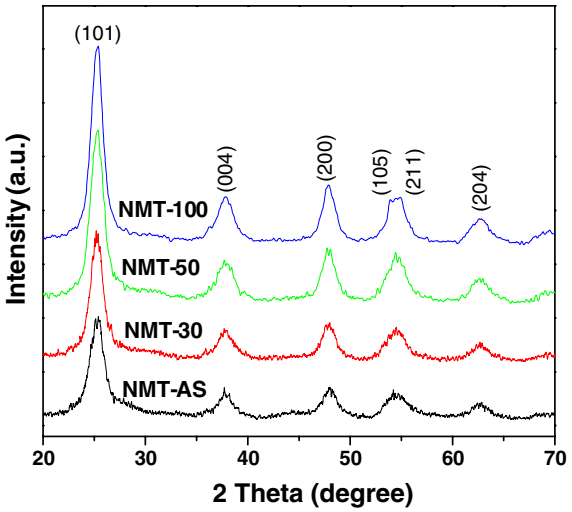

Fig. 1. XRD patterns of various NMT samples.

in Fig. 1, all NMT samples display well-defined diffraction peaks characteristic of anatase phase. After UV-illumination treatment, the crystallinity of NMT materials is markedly increased (indicated by the intensification of the diffraction peaks). Moreover, an almost unchanged crystallite size (from ca. 4.7 to 5.7 nm, see Table 1) is identified for the anatase nanocrystals in all NMT materials. By using the XRD (101) peak of a well-crystallized material obtained by calcination the NMT-AS sample at 400 °C for 8 h as Ref. [14], the relative intensities of all present low temperature-derived NMT materials is summarized in Table 1. To our knowledge, the low temperature synthesis of highly crystalline mesoporous TiO_2 material predominantly in the anatase phase via such simple UV-illumination associated low temperature strategy has not been reported. There is only the anatase phase without any rutile or brookite phase, which contrasts with the solvothermal nonhydrolytic reaction between $TiCl_4$ and

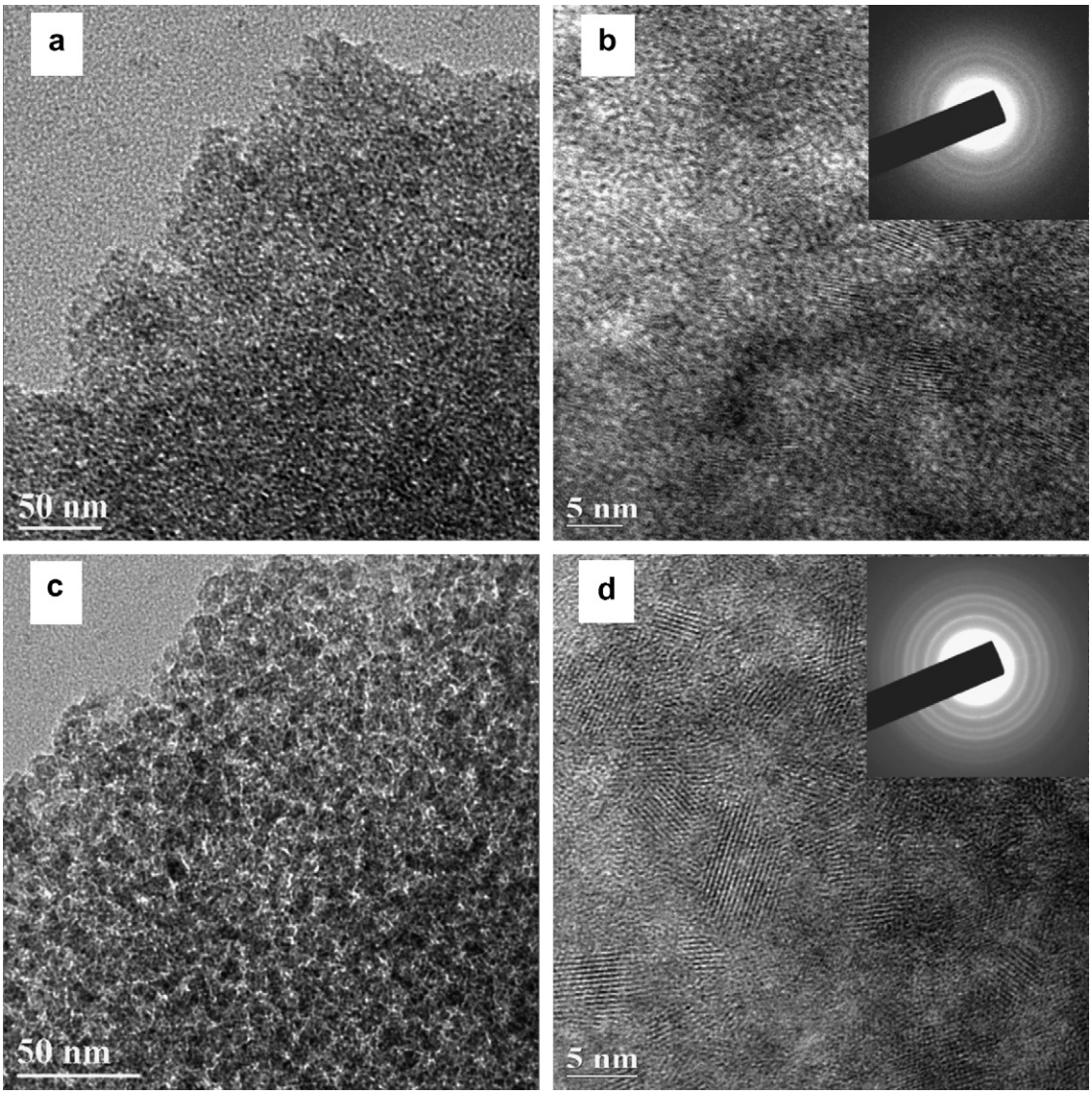

Fig. 2. TEM images of sample NMT-AS (a,b) and NMT-50 (c,d).

tert-butyl alcohol previously reported by Vioux et al. [9], where they observed both brookite and rutile phases.

The N_2 adsorption/desorption as well as the pore size distribution measurements (not shown) of the as-synthesized NMT sample reveals a well-developed mesoporous structure of the present NMT materials, which exhibits a narrow pore size distribution in the range of 3–5 nm. The specific surface area (S_{BET}) of the NMT-AS sample was found to be ca. 188 $m^2\ g^{-1}$, much higher than the reported one obtained by conventional nonhydrolytic sol–gel method [8]. Notably, a significant increase in the surface area values with respect to that of the fresh NMT-AS material is identified for the UV-illuminated samples, most likely due to the effective removal of surface organic species as confirmed by FTIR spectroscopy (not shown). Particularly noteworthy is that the well-crystalline NMT-100 sample shows a high surface area up to 269 $m^2\ g^{-1}$, which is among the highest of reported highly crystalline TiO_2 materials [5,10]. By assuming the nanocrystalline anatase particles to be spherical and considering the density of titania as 3.9 g cm^{-3}, the average crystallite size for the NMT-100 sample was calculated as 5.7 nm according to the surface area, which matched very well with the data calculated from XRD measurement.

The TEM images reveal a high dispersion of all present NMT materials, as shown in Fig. 2a and c. It is seen that the disordered mesostructure of the NMT samples is due to the aggregation of the nanosized TiO_2 particles [15]. Images at higher magnification (Fig. 2b and d) reveal that the product consists of loosely aggregated nanocrystallites of 4–6 nm in average size, which may account for the presence of well-defined mesopores as observed in the N_2 adsorption measurements. Additionally, the selected-area electron diffraction (SAED) patterns attached to Fig. 2b and d show sets of diffraction rings indexed to anatase, giving evidence the polycrystalline nature for both NMT-AS and NMT-50 samples. It is also noticeable that the presence of appreciable amount of amorphous domains in Fig. 2b makes it rather difficult to distinguish the boundaries of the particles clearly, showing the inherently semicrystalline nature of the NMT-AS sample. Noteworthy is that well-defined lattice fringes along with a pronounced intensification in the SAED patterns is observed for the NMT-50 sample, thus further confirming a pronounced enhancement in the crystalline degree upon UV-illumination.

The effect of post UV-illumination on the surface characteristics of the NMT samples was further investigated by XPS characterization. From the O 1s photoemission spectra as shown in Fig. 3a, one can see an additional signal at ca. 532.6 eV indicative of the surface hydroxyl groups (O_{OH}) besides the main peak at 530.2 eV corresponding to lattice oxygen (O_L) in TiO_2 [16]. Moreover, the presence of appreciable amount of Ti^{3+} species pointing to the formation of surface oxygen vacancies has been identified in the illuminated NMT samples (Fig. 3b), which is believed to be favorable for the generation of surface hydroxyl

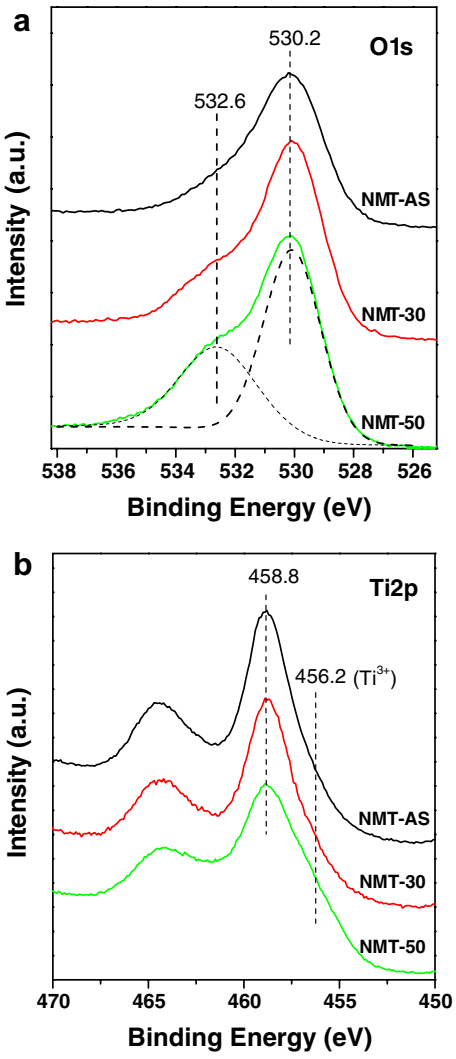

Fig. 3. O1s (a) and Ti2p (b) photoemission XPS spectra of various NMT samples.

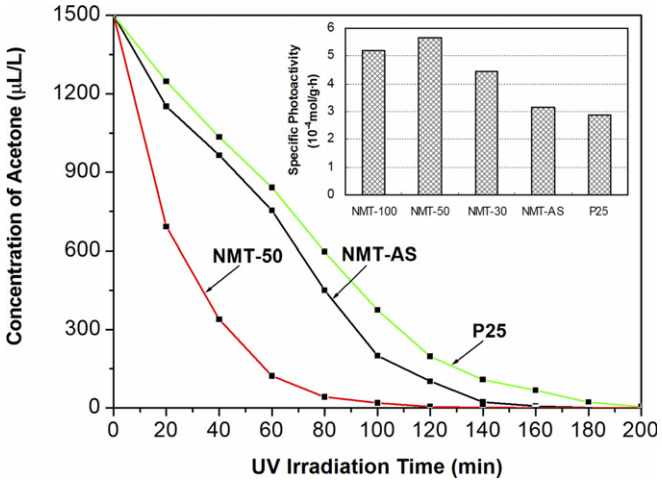

Fig. 4. Photocatalytic performances of various NMT samples. (The inset shows the average degradation rate of acetone after reaction for 1 h).

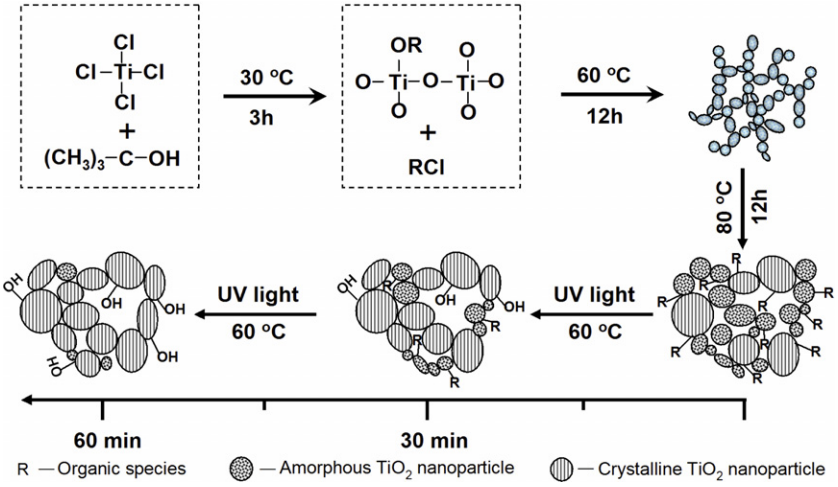

Fig. 5. Schematic illustration of the formation mechanism of the nanocrystalline mesostructured TiO_2 (NMT) material via the present integrated low temperature strategy.

groups (O_{OH}) [17]. Based on the peak area analysis, the ratios of O_{OH} to O_T ($O_T = O_{OH} + O_L$) for NMT samples with the UV-illumination time from 0 to 100 min was calculated [18]. As shown in Table 1, the ratio of O_{OH}/O_T increases continuously with prolonged UV-illumination. This demonstrates that, besides the elimination of surface organic species, the post UV-illumination plays a key role in provoking the creation of surface hydroxyl species in NMT samples. Such Ti-bonded OH groups are favorable for generating and maintaining the photocatalytic activity [19].

Acetone was used as the probe reactant to examine the photocatalytic oxidation activities of commercial Degussa P-25 and the present NMT samples. As shown in Fig. 4, all NMT samples show much higher photocatalytic activities than the Degussa P-25 photocatalyst. The excellent photocatalytic activity of the NMT samples could be attributed to the well-crystalline anatase phase which facilitates the transfer of photo-induced holes from bulk to surface for oxidation of acetone and also effectively inhibits the re-combination between the photo-induced holes and electrons which may enhance the quantum yield [5,20]. Meanwhile, the high activity could also be related to the well-defined mesoporous structure with a high surface area which can promote the diffusion and adsorption of acetone molecules on the catalyst [21]. Moreover, from the inset to Fig. 4, it is obvious that the highest photoactivity is obtained with the sample NMT-50, despite a relatively lower crystallinity and surface area as compared to the NMT-100 material. It is likely that, apart from the high surface area and well-crystallized anatase phase, the presence of an optimal amount of surface carbonaceous residues (as determined by TG analysis, Table 1) also plays an important role in the photocatalytic performance of the present NMT materials [21,22].

Previous investigations concerning the photochemical treatment of microporous or mesoporous silica materials at near room temperature conditions reveal, that non-thermal calcination by short-wavelength UV irradiation (184–257 nm) may result in complete low-temperature elimination of organic structure-directing agents, thus leading to a better reservation of the overall framework integrity with respect to conventional thermal calcination [23,24]. For the present nonhydrolytic-derived NMT-AS material comprising organic-capped semicrystalline nanocrystals, on exposure to a longer wavelength UV light in air, an effective removal of surface organic species along with the generation of oxygen vacancies thereby inducing the beneficial formation of surface Ti–OH groups occurs. Moreover, a pronounced microstructural rearrangement leading to the transformation from semicrystalline to crystallized anatase phase accompanied by the above "self-oxidation" photochemical effect is possible for the NMT materials during the present UV-illumination processing (see Fig. 5). This may well account for the prominent increase in the crystallization degree without experiencing any sintering or significant growth of the anatase grains in the NMT materials and the significant increase in catalytic activity as a function of nonhydrolytic-derived precursor UV processing. In this respect, the low temperature UV processing of the nonhydrolytic-derived nanocrystalline TiO_2 can provide unique opportunity for generating highly crystalline mesoporous TiO_2 with favorable microstructural and surface modifications.

4. Conclusion

In conclusion, a simple low temperature method has been successfully developed for the synthesis of highly effective nanocrystalline mesostructured TiO_2 photocatalysts with pure anatase phase and a high specific surface area via an integrated nonhydrolytic sol–gel/UV-illumination strategy. The particular structural features of the present NMT materials, with tailored crystallinity and surface properties achievable during a low temperature process

may find applications in other technologically important fields such as solar energy conversion and sensors.

Acknowledgements

The financial supports from National Science Foundation of China (Grant Nos. 20473021, 20421303, 20503005 and 20407006), the National Basic Research Program of China (Grant No. 2003CB615807) and the Research Fund for the Doctoral Program of Higher Education (Grant No. 20050246071) are gratefully acknowledged.

References

[1] A. Fujishima, T.N. Rao, D.A. Tryk, J. Photochem. Photobiol. C: Photochem. Rev. 1 (2000) 1.
[2] M.R. Hoffmann, S.T. Martin, C. Wonyong, D.W. Bahnemannt, Chem. Rev. 95 (1995) 69.
[3] A.L. Linsebigler, G. Lu, J.T. Yates Jr., Chem. Rev. 95 (1995) 735.
[4] J.C. Yu, J.G. Yu, L.Z. Zhang, W. Ho, J. Photochem. Photobiol. A 148 (2002) 263.
[5] H.X. Li, G.S. Li, J. Zhu, Y. Wan, J. Mol. Catal. A 226 (2005) 93.
[6] J.G. Yu, J.C. Yu, W. Ho, M.K. Leung, B. Cheng, G.K. Zhang, X. Zhao, J. Appl. Catal. A 255 (2003) 309.
[7] D. Holzinger, G. Kickelbick, Chem. Mater. 15 (2003) 4944.
[8] G.Q. Guo, J.K. Whitesell, M.A. Fox, J. Phys. Chem. B 109 (2005) 18781.
[9] P. Arnal, R.J.P. Corriu, D. Leclercq, P.H. Mutin, A. Vioux, J. Mater. Chem. 6 (1996) 1925.
[10] C.C. Wang, J.Y. Ying, Chem. Mater. 11 (1999) 3113.
[11] C. Su, B.Y. Hong, C.M. Tseng, Catal. Today 96 (2004) 119.
[12] K. Hashimoto, K. Wasada, N. Toukai, H. Kominami, Y. Kera, J. Photochem. Photobiol. A 136 (2000) 103.
[13] J. Joo, S.G. Kwon, T. Yu, M. Cho, J. Lee, J. Yoon, T. Hyeon, J. Phys. Chem. B 109 (2005) 15297.
[14] B. Ohtani, Y. Ogawa, S.I. Nishimoto, J. Phys. Chem. B 101 (1997) 3746.
[15] K. Yoo, H. Choi, D.D. Dionysiou, Chem. Commun. (2004) 2000.
[16] H.M. Liu, W.S. Yang, Y. Ma, Y. Cao, J.N. Yao, J. Zhang, T.D. Hu, Langmuir 19 (2003) 3001.
[17] X.Y. Liu, X.B. Zhao, Appl. Phys. Lett. 88 (2006) 013905.
[18] H. Jensen, A. Soloviev, Z.S. Li, E.G. Sogaard, Appl. Surf. Sci. 246 (2005) 239.
[19] Q.J. Yang, C. Xie, Z.L. Xu, Z.M. Gao, Y.G. Du, J. Phys. Chem. B 109 (2005) 5554.
[20] H.X. Li, J. Li, Y. Huo, J. Phys. Chem. B 110 (2006) 1559.
[21] Y. Yu, J.C. Yu, C. Chan, Y. Che, J.C. Zhao, L. Ding, W.K. Ge, P.K. Wong, Appl. Catal. B 61 (2005) 1.
[22] P.D. Cozzoli, R. Comparelli, E. Fanizza, M.L. Curri, A. Agostiano, Mater. Sci. Eng. C 23 (2003) 707.
[23] A. Hozumi, Y. Yokogawa, T. Kameyama, K. Hiraku, H. Sugimura, O. Takai, M. Okido, Adv. Mater. 12 (2000) 985.
[24] A.N. Parikh, A. Navrotsky, Q. Li, C.K. Yee, M.L. Amweg, A. Corma, Micropor. Mesopor. Mater. 76 (2004) 17.